

Direct Detection of Type II-P Supernova Progenitors with the *Euclid* and CSST Surveys

Junjie Wu^{1,2}, Ning-Chen Sun^{2,1,3,★}, Zexi Niu^{2,1}, Tianmang Zhang^{1,2}, Chun Chen^{4,5,6}, Xiaohan Chen^{7,1}, Nancy Elias-Rosa^{8,9}, Morgan Fraser¹⁰, Xinyi Hong^{2,1}, Justyn Maund¹¹, César Rojas-Bravo^{2,1}, Anyu Wang^{2,1}, Beichuan Wang¹, Ziyang Wang^{2,1}, Qiang Xi^{2,1}, Linxi Zhang^{2,1}, and Yinuo Zhang^{1,2}

¹ National Astronomical Observatories, Chinese Academy of Sciences, Beijing, 100101, China

² School of Astronomy and Space Science, University of Chinese Academy of Sciences, Beijing, 100049, China

³ Institute for Frontiers in Astronomy and Astrophysics, Beijing Normal University, Beijing, 102206, China

⁴ School of Physics and Astronomy, Sun Yat-sen University, Zhuhai, 519082, China

⁵ CSST Science Center for the Guangdong-Hong Kong-Macau Greater Bay Area, Sun Yat-sen University, Zhuhai, 519082, China

⁶ Dipartimento di Fisica, Università di Napoli "Federico II", Compl. Univ. di Monte S. Angelo, Via Cinthia, Napoli, I-80126, Italy

⁷ School of Physics and Astronomy, China West Normal University, Nanchong, 637002, China

⁸ INAF – Osservatorio Astronomico di Padova, vicolo dell'Osservatorio 5, Padova, 35122, Italy

⁹ Institute of Space Sciences (ICE, CSIC), Campus UAB, Carrer de Can Magrans s/n, Barcelona, 08193, Spain

¹⁰ School of Physics, University College Dublin, L.M.I. Main Building, Beech Hill Road, Dublin 4, D04 P7W1, Ireland

¹¹ Department of Physics, Royal Holloway, University of London, Egham, TW20 0EX, United Kingdom

Received January xx, 2026

ABSTRACT

Context. A central goal in supernova (SN) research is to identify and characterize their progenitor stars. However, this is very difficult due to the very limited archival images with sufficient depth and spatial resolution required for direct progenitor detection and due to the circumstellar dust which often biases the estimate of their intrinsic parameters. This field will be revolutionized by *Euclid* and the upcoming Chinese Space Station Survey Telescope (CSST), which will conduct deep, wide-field, high-resolution and multi-band imaging surveys.

Aims. We aim to evaluate the capability of *Euclid* and CSST to detect and characterize the red supergiant (RSG) progenitors of Type II-P SNe.

Methods. We analyze the detection capability by comparing the model magnitudes of RSG progenitors with the detection limits under different conditions of distance, extinction and host-galaxy background, and we estimate the annual detection rates with Monte-Carlo simulations. We explore how to recover the intrinsic properties of SN progenitors with the help of radiation transfer calculations in circumstellar dust.

Results. We find the optical and near-infrared filters of the *Euclid* and CSST are highly effective for detecting RSG progenitors. We predict that archival images from the completed *Euclid* and CSST surveys will enable $\lesssim 13$ (or 24) progenitor detections per year within the mass range of $8\text{--}16$ (or $8\text{--}25$) M_{\odot} , an order of magnitude higher than the current detection rate of ~ 1 detection per year (primarily based on HST). In the presence of circumstellar dust, the emerging spectral energy distribution (SED) of the SN progenitor is mainly affected by the optical depth and is almost independent of dust temperature in the *Euclid* and CSST filters. Our mock tests demonstrate that one can derive the progenitor mass and dust optical depth simultaneously by fitting the observed SED over the 11 filters of *Euclid* and CSST surveys while fixing the dust temperature to a typical value.

Conclusions. *Euclid* and CSST will significantly enlarge the sample of direct progenitor detections with accurate mass measurements, which is crucial to resolve the long-standing RSG problem.

Key words. Stars: massive – supergiants – Surveys – Stars: fundamental parameters – Stars: evolution – supernovae: general

1. Introduction

Core-collapse supernovae (CCSNe), the explosive deaths of massive stars, play a vital role in shaping galaxies through chemical enrichment, feedback into the interstellar medium, and the formation of compact remnants such as neutron stars and black holes. They also serve as critical laboratories for testing theories of massive star evolution and as multi-messenger sources of neutrinos, gravitational waves, and cosmic rays (Warren et al. 2020). It is a central goal in SN research to identify and characterize SN progenitors. Direct progenitor detection by comparing pre-explosion images with post-explosion

observations has so far yielded only a handful of confirmed cases, primarily from archival *Hubble* Space Telescope (HST) data (e.g., Kilpatrick & Foley 2018; Kilpatrick et al. 2021, 2023; Maund et al. 2005, 2011, 2014; Niu et al. 2023, 2024, 2025; Smartt 2009; Van Dyk et al. 2014, 2019, 2024; Xiang et al. 2019, 2024a,b).

These observations have revealed red supergiant (RSG) progenitors for the majority of Type II-P SNe, yet all measured initial masses fall below $\sim 16\text{--}18 M_{\odot}$, despite stellar evolution models predicting that RSGs can exist up to $\sim 25\text{--}30 M_{\odot}$ (Smartt 2015). This discrepancy, commonly referred to as the "RSG problem", remains unresolved in massive star evolution. It is possible that the most massive RSGs

* E-mail: sunnc@ucas.ac.cn

($M \gtrsim 18 M_{\odot}$) do not produce typical Type II-P SNe. Instead, they may explode as other types of SNe (e.g., Type II-L, Type IIn or Type II-b) (Leonard 2011; Groh et al. 2013; Suzuki & Shigeyama 2025) or may not yield a visible transient at all. In the latter case, these stars could undergo failed explosions, collapsing directly into black holes without a bright signal, due to insufficient energy in the neutrino-driven revival of the stalled shock (Nadezhin 1980; Lovegrove & Woosley 2013; Kashiyama & Quataert 2015; Sukhbold et al. 2016). Therefore, study of the RSG problem is crucial to our understanding of the final fate of massive stars and their explosion physics.

The current sample of detected Type II-P SN progenitors, however, remains extremely small (fewer than 30 secure identifications), raising concerns about the statistical significance of the RSG problem. With such limited numbers, the apparent upper mass cutoff could simply reflect sampling variance rather than a true physical boundary (Davies & Beasor 2018). Moreover, circumstellar dust formed in pre-explosion mass-loss episodes can cause significant, wavelength-dependent extinction that is not accounted for in standard foreground-only extinction corrections (Walmswell & Eldridge 2012). If uncorrected, this extra dimming leads to underestimates of progenitor luminosities and, consequently, initial masses derived from evolutionary tracks.

Therefore, it is very important to build a large sample of direct progenitor detections with well-determined progenitor parameters. Currently, the scarcity of progenitor detections stems from stringent observational requirements: deep, high-resolution images of nearby galaxies before explosion. HST, while offering excellent resolution, covers only a tiny fraction of the sky, severely limiting the number of observed galaxies and thus the yield of detectable progenitors. Moreover, progenitors identified in archival HST images are frequently detected in only one or two filters, providing insufficient spectral information to reliably constrain circumstellar extinction. In many cases, the circumstellar extinction is highly uncertain, and often implicitly assumed to be zero, despite significant dust formation often occurring in the dense winds of massive stars.

This field will be revolutionized by the advent of the *Euclid* mission and the Chinese Space Station Survey Telescope (CSST). *Euclid* is a medium-class mission in the European Space Agency's (ESA) Cosmic Vision 2015–2025 programme, launched in July 2023. Operating from the Sun–Earth L2 Lagrange point, it carries a 1.2-meter telescope equipped with two main scientific instruments: the visible imaging instrument (VIS) and the Near Infrared Spectrometer and Photometer (NISP). VIS delivers high-resolution optical imaging in the *I*-band over a 0.54 deg^2 field of view (FoV) with $0.1'' \text{ pixel}^{-1}$ (*Euclid* Collaboration et al. 2025a), while NISP provides near-infrared (NIR) imaging in *Y*, *J*, *H* bands over a 0.57 deg^2 FoV with $0.3'' \text{ pixel}^{-1}$ and slitless spectroscopy (*Euclid* Collaboration et al. 2025b). Over its nominal 6-year mission, *Euclid* will conduct the *Euclid* Wide Survey (EWS), covering $14\,679 \text{ deg}^2$ (or $13,245 \text{ deg}^2$ due to the optical stray light problem) of extragalactic sky with unprecedented depth ($I = 26.3$, $Y = 24.6$, $J = 24.6$, $H = 24.5$ AB mag for 5σ point source; *Euclid* Collaboration et al. 2025a,b) and spatial resolution of $0.13''$, $0.33''$, $0.35''$, and $0.35''$ in the respective bands (*Euclid* Collaboration et al. 2025c).

Complementing *Euclid* in the ultraviolet (UV) and optical domains, the upcoming CSST promises a similarly transformative advance. Scheduled for launch in 2027, CSST features an off-axis three-mirror anastigmat (TMA) design with a 2-meter primary mirror and carries five main scientific instruments. It will conduct a deep, multi-band imaging survey across seven

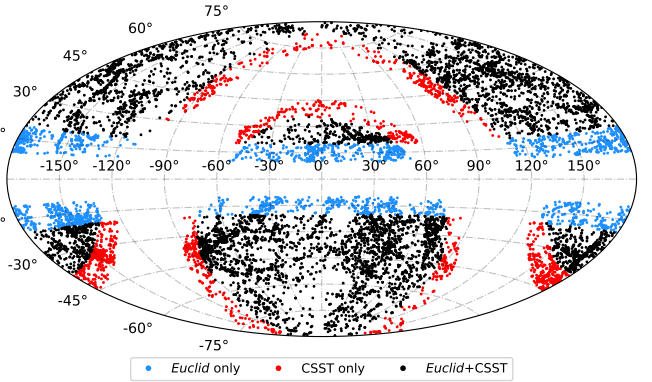


Fig. 1: Local galaxies within the *Euclid* and CSST survey footprints, shown in barycentric mean ecliptic coordinates. Galaxies within the *Euclid*+CSST area are marked in black, those within the *Euclid*-only area in blue, and those within the CSST-only area in red.

photometric bands ($NUV = 25.4$, $u = 25.4$, $g = 26.3$, $r = 26.0$, $i = 25.9$, $z = 25.2$, and $y = 24.4$ AB mag for 5σ point source) over a wide FoV of 1.1 deg^2 with $0.074'' \text{ pixel}^{-1}$, achieving a spatial resolution of $\sim 0.20''$, ultimately covering up to $17\,500 \text{ deg}^2$ of the sky over a 10-year life cycle (CSST Collaboration et al. 2025; Ban et al. 2025; Wei et al. 2025). CSST will operate in a co-orbit with the China Space Station (CSS) at an altitude of approximately 400 km. This unique orbital configuration allows CSST to periodically rendezvous and dock with the CSS for on-orbit servicing (OOS), enabling instrument upgrades, maintenance, and repairs, thereby ensuring long-term operational flexibility and scientific longevity (Zhan 2011, 2021).

While the primary science goals of *Euclid* and CSST lie in cosmology, they also offer valuable opportunities for the identification of SN progenitors in the nearby galaxies of the local universe. These surveys will provide high-resolution images over a large sky area of $17\,500 \text{ deg}^2$. Based on this legacy dataset, SN progenitor searches will be possible for a much larger number of nearby galaxies than before (see Fig. 1). Moreover, the *Euclid* and CSST will perform their surveys in a total of 11 filters in the UV, optical and NIR bands, covering a very wide wavelength range from $\sim 2000 \text{ \AA}$ to $\sim 20\,000 \text{ \AA}$. This will tightly constrain the spectral energy distribution (SED) of the SN progenitors, allowing for accurate determination of their properties (see Fig. 2).

In this work, we assess the capability of the *Euclid* and CSST surveys in detecting Type II-P SN progenitors and explore how to derive their fundamental parameters based on these detections. This paper is structured as follows. In Section 2 we compare the brightness of SN progenitors with the detection limits of *Euclid* and CSST to estimate the number of progenitors detections each year. Section 3 analyzes the influence of circumstellar extinction on the observed SED and presents a possible method to constrain progenitor mass in the presence of circumstellar extinction. This paper is finally closed with a summary and conclusions.

2. Detection Capability for RSG Progenitors

2.1. Detection Limits

It is very important to assess the detection capability for CCSN progenitors by *Euclid* and CSST surveys. For simplic-

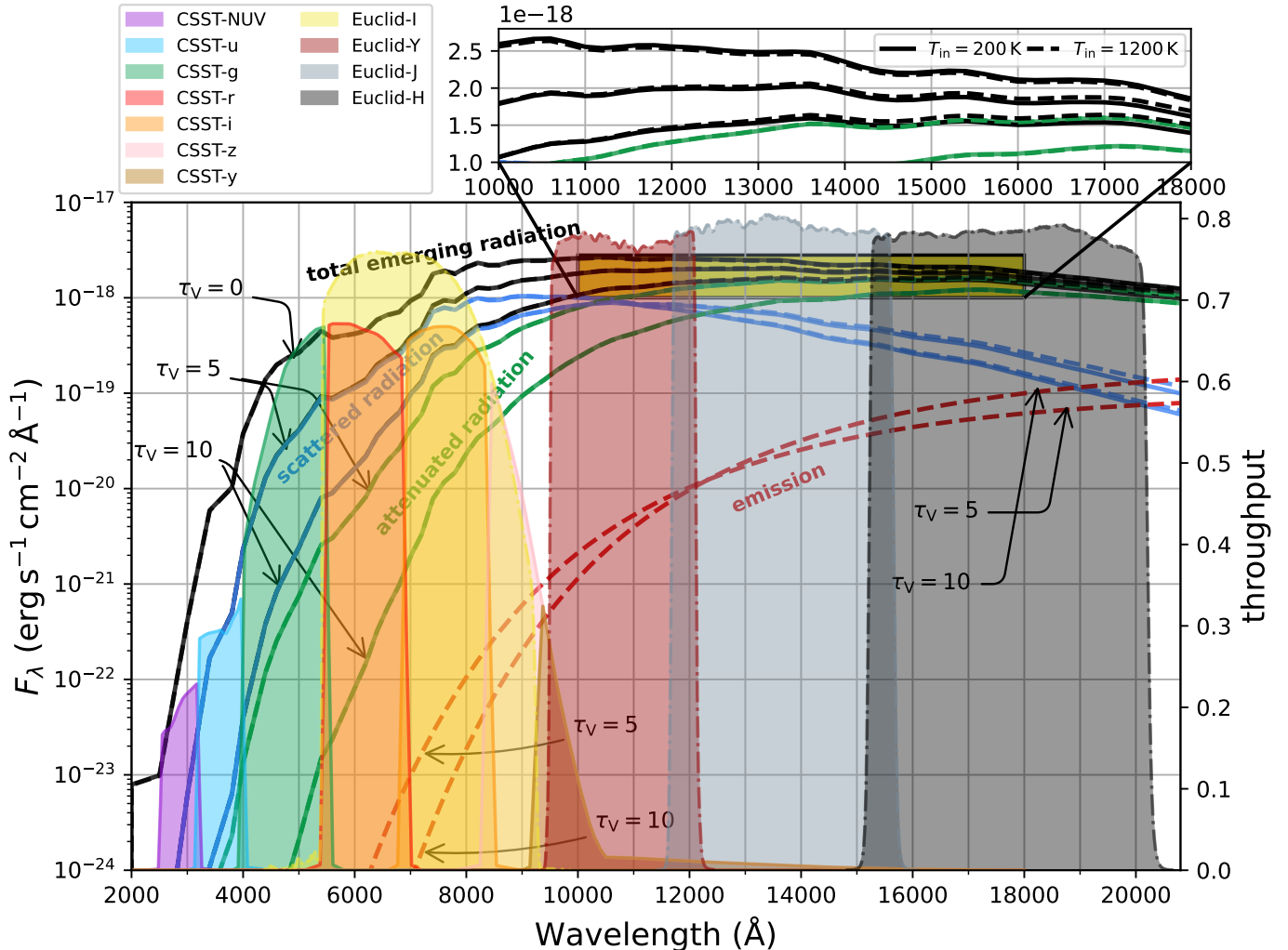


Fig. 2: Sensitivity curves for the filters of the *Euclid* and CSST surveys, along with synthetic SEDs for an RSG with initial mass $M_{\text{ini}} = 15 M_{\odot}$, surrounded by varying degrees of O-rich dust, distributed in a spherical envelope. Colored shaded regions display the total sensitivity of photometric bands in the *Euclid* and CSST surveys. Solid lines represent the dust with an inner temperature $T_{\text{in}} = 200 \text{ K}$ and dashed lines show the $T_{\text{in}} = 1200 \text{ K}$ condition. Black, blue, green and red lines with optical depth (τ_V) annotations correspond to the total emerging radiation, scattered radiation, attenuated radiation and the dust emission, respectively. Dust emission for $T_{\text{in}} = 200 \text{ K}$ is much lower than the extent of the y-axis. The flux densities shown are obtained assuming the RSG is located at a distance of $d = 10 \text{ Mpc}$.

ity, we firstly consider CCSN progenitors at a distance of $d = 10 \text{ Mpc}$ without any extinction or host-galaxy background. Subsequently, we develop exposure time calculators for determining the signal-to-noise ratio (SNR) and limiting magnitude of point sources based on the photometric parameters of *Euclid* and CSST surveys (Euclid Collaboration et al. 2025c; CSST Collaboration et al. 2025). Fig. 3 shows the PARSEC (V2.1; Bressan et al. 2012; Chen et al. 2014, 2015; Fu et al. 2018) evolutionary tracks for solar-metallicity massive stars in comparison to the *Euclid*/CSST 5σ detection limits under such conditions. Here we have assumed a blackbody SED and calculate the synthetic magnitudes with the PYSPHOT package (STScI Development Team 2013). In the PARSEC models, massive stars up to $30 M_{\odot}$ evolve to RSGs before CCSNe, while those above $30 M_{\odot}$ become Wolf-Rayet (WR) stars. Some observational studies suggest that the turn-off mass required to produce WN stars (nitrogen-sequence WR stars) is at least $25 M_{\odot}$ in the Milky Way, rising to above $30 M_{\odot}$ in the Large Magel-

lanic Cloud, and is likely closer to $35\text{--}40 M_{\odot}$ for the formation of WC stars (carbon-sequence WR stars) (Massey et al. 2001; Massey & Olsen 2003; Crowther 2007; Smartt 2009). It is worth noting that the precise boundary between RSG and WR stars can be critically affected by the highly uncertain mass-loss prescription in stellar models (Woosley et al. 2002; Heger et al. 2003; Levesque et al. 2005, 2006).

Most of the RSG progenitors fall below the 5σ detection limits of both the *NUV* and *u* filters of CSST; only the extremely massive RSG progenitors with $M_{\text{ini}} \sim 30 M_{\odot}$ (or $\sim 24 M_{\odot}$) marginally exceed the *NUV*-band (or *u*-band) limit. This is because the RSG progenitors have very low effective temperatures (3,300–4,000 K; Smartt 2015) and most of their radiation lies at long wavelengths (see Fig. 2). The other optical and NIR filters, on the contrary, are very useful in probing the cool RSGs. At $d = 10 \text{ Mpc}$ and without extinction or host-galaxy background, these filters can detect RSG progenitors even down to the lowest mass limit for CCSNe of $M_{\text{ini}} = 8 M_{\odot}$.

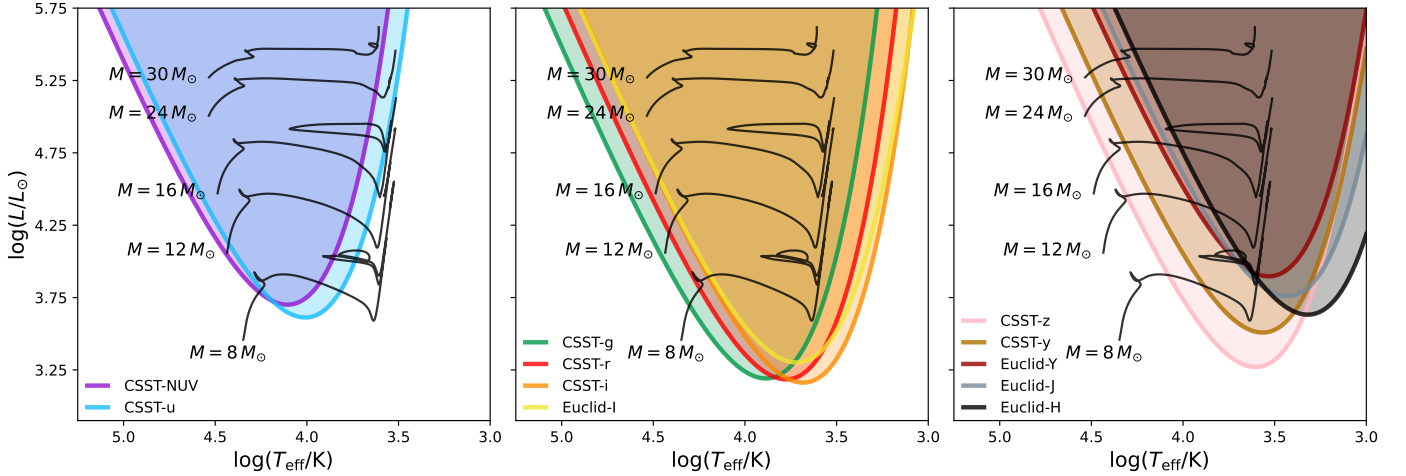


Fig. 3: The evolutionary tracks of massive stars in comparison to the *Euclid*/CSST detection limits. Black solid lines show the evolutionary tracks of massive stars with initial masses of 8, 12, 16, 24, and $30 M_{\odot}$ obtained from the PARSEC stellar evolution models. Colored solid curves indicate the typical detection limits for the *Euclid* and CSST surveys.

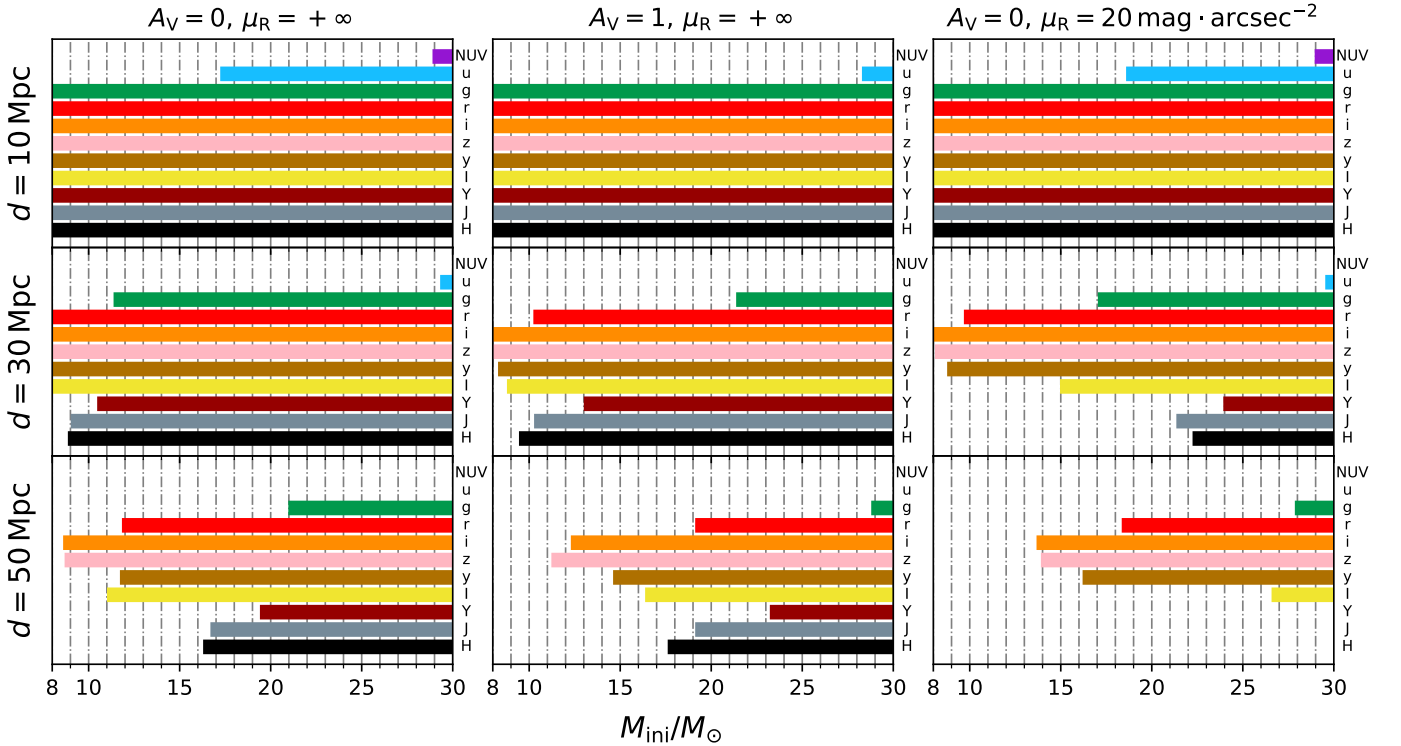


Fig. 4: Mass range of SN progenitors detectable by *Euclid* and CSST surveys. This figure is divided into nine panels. Three columns represent $A_V = 0$ with no host-galaxy background, $A_V = 1$ with no host-galaxy background, and $A_V = 0$ with a R -band background surface brightness of $20 \text{ AB mag arcsec}^{-2}$. Three rows correspond to distances of 10, 30, and 50 Mpc, respectively. Each panel illustrates the detectable mass range of SN progenitors under the specified extinction and host-galaxy background conditions.

Whether a RSG progenitor can be detected also depends on its distance and extinction, which influences its brightness in different filters, as well as the host-galaxy background, which affects the detection limits of *Euclid*/CSST. To assess their influence, we repeat the above analysis and derive the lowest mass of RSG progenitors that can be detected under different conditions (see Fig. 4). In this context, a detection is defined as the identification of a source in at least one photometric band with $\text{SNR} \geq 5$. We consider three different distances of $d = 10, 30, 50 \text{ Mpc}$.

For extinction, we consider $A_V = 0$ and 1 mag and use a standard extinction law of Cardelli et al. (1989) with $R_V = 3.1$. For host-galaxy background, we consider an R -band surface brightness of $\mu_R = +\infty$ (i.e., no background) and $20 \text{ mag arcsec}^{-2}$; we calculate the surface brightnesses in the other filters by assuming an SED of a typical Sb spiral galaxy from the SWIRE library (Polletta et al. 2007), with which we re-derive the detection limits of *Euclid*/CSST.

As previously mentioned, at $d = 10$ Mpc without extinction or host-galaxy background the lowest-mass RSG progenitor with $M_{\text{ini}} = 8.0 M_{\odot}$ can be detected in all *Euclid*/CSST filters except the very blue *NUV* and *u* bands. At 30 Mpc, an $8-M_{\odot}$ progenitor is still detectable in the *r*, *i*, *z*, *y*, *I* bands and its brightness falls below the detection limits of all other filters. Now the *g* band can detect down to $M_{\text{ini}} = 11.8 M_{\odot}$. At 50 Mpc, an $8-M_{\odot}$ progenitor is no longer detectable, and $9.0 M_{\odot}$ is the lowest mass of RSG progenitors that can be detected in at least one filter (the *i* band) while detection in the *z* band requires a slightly higher initial mass of $9.1 M_{\odot}$.

At $d = 10$ Mpc, the effect of extinction is not very obvious since at such a close distance the RSG progenitors are very bright even with a higher extinction. An $8-M_{\odot}$ progenitor can still be detected in most of the filters. At larger distances, the effect of extinction becomes pronounced for the bluer filters. For instance, at 30 Mpc, the *g* band can only detect down to $21.8 M_{\odot}$ with $A_V = 1$ mag compared with $11.8 M_{\odot}$ without extinction. Extinction hardly affects the redder, in particular the NIR filters. For instance, at $d = 50$ Mpc and $A_V = 1$ mag, the lowest mass to be detected in the *J* and *H* bands only slightly increase to 19.5 and $18.0 M_{\odot}$ from 17.1 and $16.7 M_{\odot}$ ($A_V = 0$), respectively, due to their low extinction coefficients ($A_J/A_V \approx 0.25$, $A_H/A_V \approx 0.17$).

Increasing the host-galaxy background degrades the detection limits of point sources by *Euclid*/CSST. At $d = 10$ Mpc, the effect of such a surface brightness is not obvious since at such a close distance the RSG progenitors are very bright. At $d = 30$ Mpc, the lowest detectable masses in the *g*, *r*, *i*, *z*, *y* bands are 17.4 , 10.1 , 8.4 , 8.5 , and $9.2 M_{\odot}$, indicating that these bands still offer strong detection capabilities. In the *Y*, *J* and *H* bands, however, the lowest mass to be detected increases significantly from 10.9 , 9.4 and $9.3 M_{\odot}$ (no host-galaxy background) to 24.3 , 21.7 and $22.6 M_{\odot}$, respectively, indicating that the effect of host-galaxy background becomes pronounced in the NIR filters. At $d = 50$ Mpc, even a $30-M_{\odot}$ star becomes undetectable in the *Y*, *J* and *H* bands. This wavelength-dependent effect arises primarily because, in spiral galaxies, redder bands exhibit significantly higher surface brightness than bluer bands due to the presence of a dust-rich stellar disk.

In summary, the *Euclid* and CSST filters are very useful in detecting the canonical Type II-P progenitors (i.e., single-star RSGs) except the very blue *NUV* and *u* bands. At a distance of 10 Mpc, an $8-M_{\odot}$ progenitor can be detected in all other filters in case of no extinction or host-galaxy background. With higher distance, extinction and/or host-galaxy background (e.g., scenarios involving binary evolution, enhanced circumstellar mass loss, or dense dusty envelopes), the detection capability for RSG progenitors will be partially degraded, yet detection potential remains.

Notably, in crowded stellar fields, particularly near the centers of galaxies or in dense star-forming regions, source confusion and background contamination can hinder the identification and photometric measurement of individual RSG progenitors. Overlapping on point-spread functions (PSFs) makes it difficult to disentangle the progenitor's signal from neighboring stars or diffuse emission. Thus, while the angular resolution and the filters themselves are well-suited for RSG detection, practical detectability also depends critically on the local stellar density and the effectiveness of photometric techniques in crowded environments. In this work, we do not analyze the effect of confusion with other resolved objects, which requires detailed image simulations and is beyond the scope of this work. As a result, our estimate of the detection capability is overrated.

2.2. Detection Rates

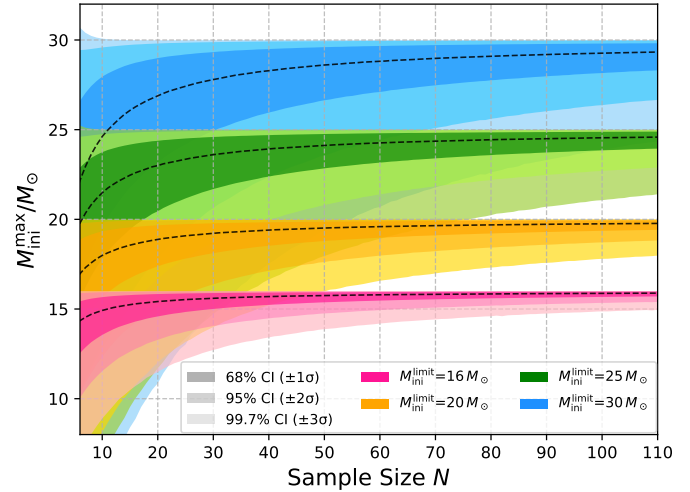


Fig. 5: Expected maximum initial masses $M_{\text{ini}}^{\text{max}}$ in SN II-P progenitor samples of varying sizes, derived with different assumed upper limits on the initial masses $M_{\text{ini}}^{\text{limit}}$ of RSGs. The pink, yellow, green, and blue shaded regions represent the uncertainty ranges for samples with $M_{\text{ini}}^{\text{limit}} = 16, 20, 25$ and $30 M_{\odot}$, respectively. Within each colored region, dashed lines indicate the median values for each sample group, and the shading intensity varies from dark to light to represent different confidence intervals (CIs): dark, medium, and light shadings reflect the 68%, 95%, and 99.7% CIs, respectively, corresponding to $\pm 1\sigma/\pm 2\sigma/\pm 3\sigma$ deviations from the median.

After assessing the detection capabilities of SN progenitors using the *Euclid* and CSST surveys, a key remaining question pertains to the detectable samples: specifically, the annual detection rate of progenitors and the scientific insights that can be derived from these samples. To estimate the annual detection rates for Type II-P SN progenitors with different assumed upper mass limits in the *Euclid* and CSST surveys, we employ Monte Carlo simulations to generate random stellar samples within the surveyed galaxies and evaluate their detectability.

Initial stellar masses are first randomly generated with a power-law index of -2.35 based on the initial mass function (IMF) by Salpeter (1955), followed by a selection process that retains only those within a specific initial mass range (such as $8\text{--}16 M_{\odot}$ or $8\text{--}25 M_{\odot}$, etc.) as Type II-P SN progenitors. These selected progenitor stars are then assigned to galaxies within the survey area of *Euclid* and CSST using the galaxies' star formation rate (SFR) as weighting factors. The galaxy catalog used in this study is from the z0MGS project (Leroy et al. 2019; z0MGS Team 2019). SFRs of galaxies are also from the z0MGS project while Galactic extinction values are calculated using DUSTMAPS package (Green 2018) based on locations from z0MGS and the two-dimensional extinction maps from Schlegel et al. (1998); Schlafly & Finkbeiner (2011).

To simulate the host-galaxy background brightness around generated SN progenitors in the survey bands of the *Euclid* and CSST, it is essential to model the radial positions of progenitor stars within a galaxy and the surface brightness profiles of galaxies for the corresponding filters. In an exponential disk model, the surface density of star formation rate typically follows $\Sigma_{\text{SFR}}(r) \propto \exp(-r/r_0)$, where r_0 is the scale length. The total star formation rate in an annulus of radius r and width dr ,

$2\pi r \Sigma_{\text{SFR}}(r) dr$, is proportional to $r \exp(-r/r_0) dr$. When normalized, this radial distribution defines a probability density function (PDF) for the radius at which a randomly selected star-forming event occurs. Introducing the dimensionless variable $x = r/r_0$, the resulting PDF is $P(x) \propto xe^{-x}$ for $x \geq 0$, which corresponds to a Gamma distribution with shape parameter $k = 2$ and scale parameter $\theta = 1$. Thus, the stellar formation radius (in units of the scale length) follows a $\text{Gamma}(2, 1)$ distribution. Based on this distribution, we simulate the radial positions of progenitor stars within the galaxies.

Next, to determine the background brightness levels at corresponding radius in the *Euclid* and CSST filters, observed surface brightness profiles and SEDs for all galaxies within the survey footprints are required. Despite the variation of surface brightness profiles and SEDs among galaxies, there remains practical difficulty of obtaining them for large galaxy samples. Therefore, we adopt an observed surface brightness profile from a typical spiral galaxy with a matching SED template as a rough but pragmatic evaluation. Specifically, we utilize the surface brightness profile of NGC 7819 (UGC 26), a face-on Sc-type galaxy, as provided by [Gilhuly & Courteau \(2018\)](#) from the Calar Alto Legacy Integral Field Spectroscopy Area (CALIFA) survey's third data release (DR3) ([Sánchez et al. 2012](#); [Walcher et al. 2014](#); [Sánchez et al. 2016](#)). Subsequently, we apply a type Sc galaxy SED template from the SWIRE library ([Polletta et al. 2007](#)) to transform the observed SDSS *i*-band surface brightness profile into the respective survey bands of *Euclid* and CSST.

For each simulated progenitor, we adopt the effective temperature (T_{eff}) and bolometric luminosity (L_{bol}) at its final evolutionary stage from the PARSEC stellar evolution models, using the corresponding initial mass. Based on these parameters, progenitor's theoretical magnitudes are derived by interpolating from the MARCS model atmospheres ([Gustafsson et al. 2008](#)), assuming a microturbulent velocity of 5 km s^{-1} , surface gravity $\log(g) = 0$ and solar metallicity $[\text{Fe}/\text{H}] = 0$. We then determine the detection limiting magnitudes with the background brightness and the Galactic extinction for the position of each simulated progenitor and compare the limits with the progenitor's theoretical magnitudes. Based on the above analysis, we predict that, upon completion of the *Euclid* and CSST surveys, $\lesssim 13$ (or 24) Type II-P SN progenitors with the initial mass range of $8\text{--}16$ (or $8\text{--}25$) M_{\odot} will be detected annually from the archival survey images with $\text{SNR} \geq 5$.

This estimate assumes neither internal extinction within the host galaxies (including dust around the progenitor star and distributed throughout the galaxy) nor intergalactic extinction along the line of sight. However, in reality, dust extinction at all these scales will inevitably attenuate the observed flux. Such extinction not only dims the progenitor's light but also reduces the contrast between the point source and the diffuse background of its host galaxy, thereby degrading the overall detection efficiency. It is very challenging, however, to predict the internal extinction for the progenitors. Additionally, the surface brightness profile, inclination angle, and spatial distribution of dust and stars within each galaxy are highly uncertain and vary significantly from galaxy to galaxy, making it extremely challenging to accurately model or predict the resulting observational biases. Moreover, as mentioned before, source confusion is not considered in this work. Consequently, the actual detection rate of Type II-P SN progenitors is expected to be lower than our current estimate.

2.2.1. Significance of the RSG problem

Due to the limited size of observed Type II-P SN progenitor samples, it remains unclear whether the RSG problem reflects a true physical upper mass limit for progenitor stars or is instead an artifact of small-number statistics and observational biases. [Davies & Beasor \(2020\)](#) emphasized that the statistical significance of the RSG problem is between 1σ and 2σ as it could be consistent with stochastic sampling from a continuous IMF rather than a physical boundary. In the future, with a much larger sample of RSG progenitors detected by *Euclid* and CSST surveys, a key question that can be answered is the statistical significance of the upper limits on the initial masses $M_{\text{ini}}^{\text{limit}}$ of Type II-P SN progenitors.

To clarify this topic, we perform statistical simulations to show expected maximum initial masses $M_{\text{ini}}^{\text{max}}$ in progenitor samples of varying sizes. We generated initial masses of stars based on a [Salpeter \(1955\)](#) IMF and then selected progenitor samples according to different assumed upper limits on the initial masses, $M_{\text{ini}}^{\text{limit}}$, of SN II-P progenitors. From these samples, we randomly drew subsamples of varying sizes and recorded their maximum initial masses. After performing a large number of repeated samplings, we obtained the relation between the maximum initial mass and the sample size for different upper mass limits, as shown in Fig. 5.

For a sample size of $N \sim 25$ (i.e., the currently observed SN II-P progenitor sample), the maximum initial masses corresponding to different assumed upper mass limits are not significantly distinguishable. However, with a sample size of $N \gtrsim 35$, we can statistically distinguish between $M_{\text{ini}}^{\text{limit}} = 16$ and $25 M_{\odot}$ at 3σ significance. Assuming an expected practical annual detection rate of approximately 10 SN II-P progenitors, such a sample would require about 3 years to accumulate.

3. Estimating Parameters of RSG Progenitors

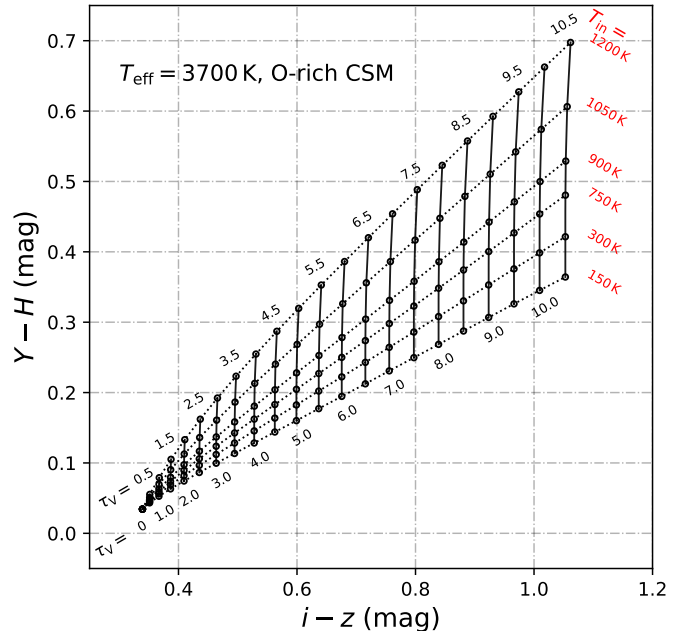


Fig. 6: $Y - H$ versus $i - z$ color-color diagram for the RSG of $T_{\text{eff}} = 3700 \text{ K}$ with O-rich circumstellar dust of different T_{in} and τ_V .

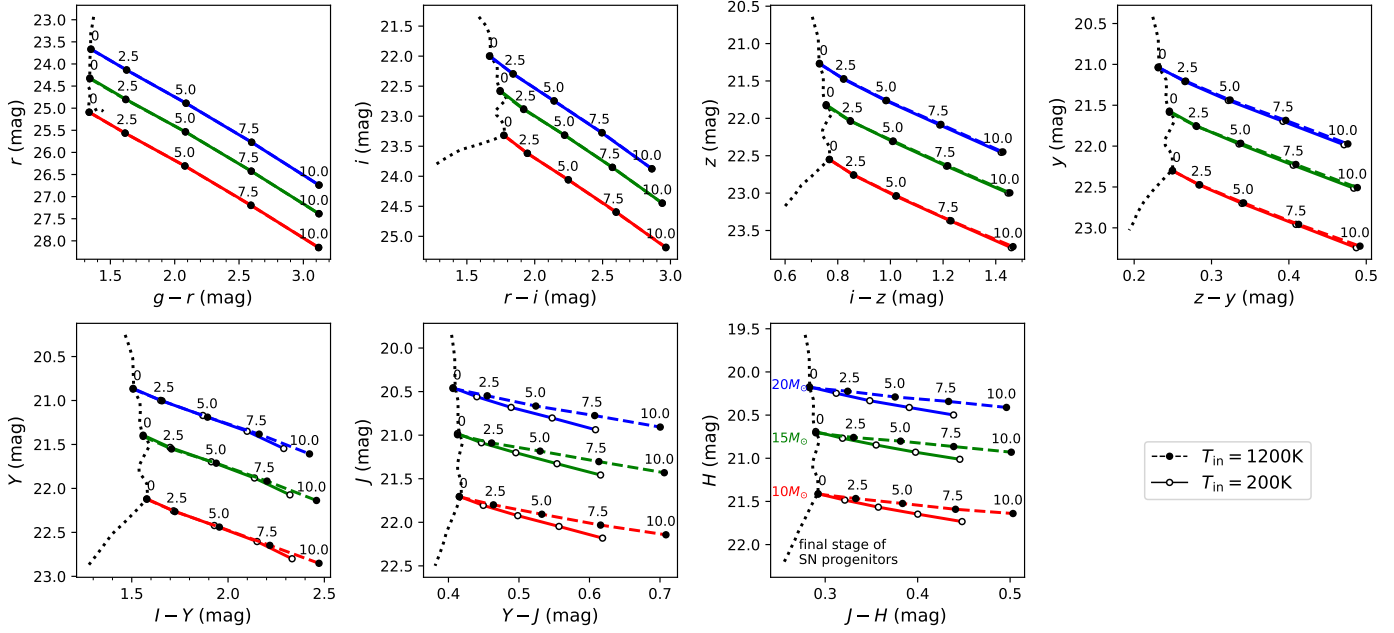


Fig. 7: Color-magnitude diagrams for RSGs with initial masses $M_{\text{ini}} = 10, 15, 20 M_{\odot}$ embedded in O-rich circumstellar dust characterized by various inner temperature T_{in} and V-band optical depth τ_V . Black dotted lines in the left portion of each panel correspond to the final stage of SN progenitors with different initial masses assuming no extinction. Colors denote the initial mass of the progenitor: red for $10 M_{\odot}$, green for $15 M_{\odot}$, and blue for $20 M_{\odot}$. Solid and dashed lines represent $T_{\text{in}} = 200$ K and $T_{\text{in}} = 1200$ K, respectively, with data points labeled with their corresponding τ_V values.

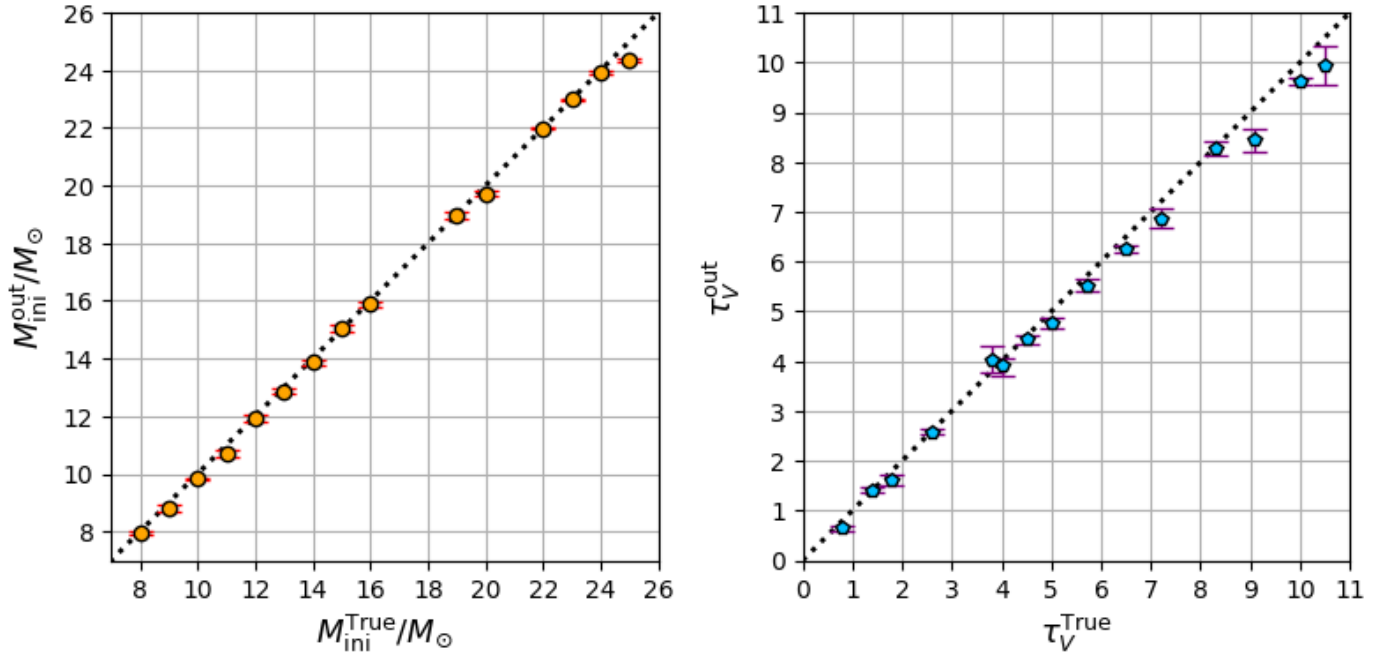


Fig. 8: Inferred parameters from MCMC fitting in comparison with the input values. *Left:* $M_{\text{ini}}^{\text{out}} / M_{\odot}$, *Right:* τ_V^{out} .

After detecting SN progenitors, it is important to derive their fundamental stellar parameters. Such parameters include the effective temperature, bolometric luminosity and the initial mass, etc. However, the existence and uncertainty of circumstellar extinction makes this difficult. Circumstellar dust plays three different roles in affecting the SED of the SN progenitor: (1) it can attenuate the stellar radiation along the line of sight via absorption and scattering (*attenuated radiation*); (2) it may scatter the stellar radiation along other directions into the line of sight, partially compensating the loss of light (*scattered radiation*); (3) it can also generate its own emission, particularly at infrared wavelengths, which is sensitive to the dust temperature (*dust emission*).

tion and scattering (*attenuated radiation*); (2) it may scatter the stellar radiation along other directions into the line of sight, partially compensating the loss of light (*scattered radiation*); (3) it can also generate its own emission, particularly at infrared wavelengths, which is sensitive to the dust temperature (*dust emission*).

To evaluate the effect of circumstellar extinction on the SED of RSG progenitors as observed by *Euclid* and CSST, we synthesize the SEDs of RSGs with an initial mass of $M_{\text{ini}} = 15 M_{\odot}$, surrounded by spherically distributed O-rich dust envelopes. For the intrinsic radiation, the effective temperature $T_{\text{eff}} = 3374 \text{ K}$ and bolometric luminosity, $\log(L_{\text{bol}}/L_{\odot}) = 5.087$, which characterize the final evolutionary stage of a $15 M_{\odot}$ progenitor, are adopted from the PARSEC stellar evolution models. We then obtain the intrinsic SED by interpolating from the MARCS model atmospheres (Gustafsson et al. 2008), assuming a microturbulent velocity of 5 km s^{-1} , surface gravity $\log(g) = 0$ and solar metallicity $[\text{Fe}/\text{H}] = 0$.

For the circumstellar dust, we assume a $\rho \propto r^{-2}$ wind-like radial density profile, a default relative thickness that is 1000 times the inner radius and a standard grain size distribution following Mathis et al. (1977), while the dust temperature at the inner boundary (T_{in}) and the V-band optical depth of the dust envelope (τ_{V}) are selected as the two free parameters to study their effects. The radiation transfer through the circumstellar dust is solved with the DUSTY (Ivezic & Elitzur 1997) code and the output SEDs are showed in Fig. 2.

From Fig. 2, it is clear that scattered radiation dominates the total emerging radiation from the *NUV* to *y* bands, attenuated radiation dominates in the *J* and *H* bands at longer wavelengths, while in the *Y* band, the scattered radiation and attenuated radiation have comparable contributions to the total emerging radiation. Both the scattered radiation and attenuated radiation are sensitive to optical depth τ_{V} and do not depend on dust temperature T_{in} . In comparison, dust emission depends on both τ_{V} and T_{in} ; however, the contribution of dust emission is very small even in the longest-wavelength *H* band ($\sim 10\%$ for $T_{\text{in}} = 1200 \text{ K}$, down to close to zero for $T_{\text{in}} = 200 \text{ K}$). As a result, the total emerging radiation is primarily dependent on the optical depth τ_{V} and is very insensitive to dust temperature T_{in} in the *Euclid* and CSST filters.

This effect is also obvious in the color-color diagram for a RSG of $T_{\text{eff}} = 3700 \text{ K}$ with O-rich circumstellar dust (see Fig. 6). As τ_{V} increases, both the $Y - H$ and $i - z$ colors become redder, reflecting the reddening effect. The $i - z$ color remains nearly constant across different values of T_{in} , while the $Y - H$ color turns redder with increasing T_{in} . This is consistent with the above analysis: dust emission, which depends on temperature, has a weak contribution only in the *H* band while in the other filters dust emission is negligible. However, even at a large τ_{V} of 10, where the color differences due to different T_{in} values are relatively pronounced, the variation in $Y - H$ color is only about 0.4 mag for T_{in} ranging from 150 K to 1200 K (which is required to be lower than 1500 K such that the dust can survive in the envelope; Pozzo et al. 2004; Sarangi et al. 2018). This difference is not very significant, considering that SN progenitors are often detected just above the detection limit and with large photometric uncertainties (e.g., Niu et al. 2023). This indicates that the circumstellar dust's T_{in} has negligible impact on the progenitor's color.

In summary, in the presence of circumstellar dust, τ_{V} controls the SED of the total emerging radiation of the SN progenitor while T_{in} has little effect for the *Euclid* and CSST filters. Based on this, we propose a new method: taking advantage of the extensive 11 filters of the *Euclid* and CSST surveys, one can fit M_{ini} and τ_{V} simultaneously by fixing T_{in} to a typical value and tracing the observed SED back to the intrinsic one. The color-magnitude diagram (see Fig. 7) demonstrates how this approach enables the recovery of the progenitor's parameters

through comparison with outputs from stellar evolution models such as PARSEC.

To validate the robustness of our new method, we conduct mock data tests by randomly generating a set of initial masses (M_{ini}), dust temperatures at the inner boundary (T_{in}) and V-band optical depths (τ_{V}) for RSGs with circumstellar dust. We simulate their multi-band photometry to generate synthetic magnitudes and add photometric uncertainties. Subsequently, we apply Markov Chain Monte Carlo (MCMC) method to perform multi-band fitting on the simulated SEDs with the inner dust temperature fixed at $T_{\text{in}} = 1000 \text{ K}$, aiming to recover the underlying physical parameters of M_{ini} and τ_{V} . As shown in Fig. 8, the inferred parameters agree remarkably well with the input values. This consistency confirms that multi-band SED fitting alone is sufficient to accurately constrain the intrinsic properties of RSG progenitors. The success can be attributed to the fact that RSGs exhibit similar intrinsic effective temperatures and photometric colors in their pre-SN stages and that their SEDs are critically dependent on M_{ini} and τ_{V} and is almost independent of T_{in} . This result strongly validates the reliability and precision of our proposed methodology.

4. Summary and Discussion

In this work, we evaluate the capability of *Euclid* and CSST surveys in detecting Type II-P SN progenitors and explore how to robustly estimate their intrinsic parameters in the presence of circumstellar dust. We find that the optical and near-infrared filters of the *Euclid* and CSST are highly effective for detecting RSG progenitors of Type II-P SNe while the very blue *NUV* and *u* bands are less useful. At a distance of 10 Mpc, an $8 M_{\odot}$ progenitor is detectable in all other filters with no extinction or host-galaxy background. However, the detectability diminishes with increasing distance, as well as in the presence of extinction and/or host-galaxy background.

Under optimistic assumptions, we predict that the archival data from the completed *Euclid* and CSST surveys will yield $\lesssim 13$ (or 24) detections of Type II-P SN progenitors per year with the initial mass range of $8-16$ (or $8-25 M_{\odot}$) at $\text{SNR} \geq 5$. This is a very optimistic estimate since we have not considered internal extinction within the host galaxy or confusion with other resolved sources. Furthermore, a progenitor sample of size $N \gtrsim 35$ would statistically distinguish between upper mass limits of $M_{\text{ini}}^{\text{limit}} = 16$ and $25 M_{\odot}$ with a significance of 3σ , which is expected to be accumulated within about 3 years.

Our analysis further demonstrates that the V-band optical depth of circumstellar dust (τ_{V}), is the dominant factor governing the SED of the total emerging radiation of SN progenitor in the *Euclid* and CSST filters, whereas the dust temperature at the inner radius (T_{in}) exerts little influence on the SED in these filters. Given that RSGs exhibit remarkably uniform effective temperatures and photometric colors during their pre-SN phases, their SEDs are primarily sensitive to M_{ini} and τ_{V} and is almost independent of T_{in} . This finding underscores the robustness of multi-band SED fitting for constraining the intrinsic properties of RSG progenitors.

Moreover, the pulsational variability of RSGs represents a critical yet often overlooked systematic uncertainty in the derivation of progenitor parameters for Type II-P SNe. These oscillations, which are commonly detected in nearby Type II-P SN progenitors such as SN 2023ixf (Niu et al. 2023; Xiang et al. 2024a) and SN 2024ggi (Xiang et al. 2024b), induce time-dependent changes in luminosity, effective temperature, and radius, directly biasing estimates of progenitor mass derived from pre-explosion

imaging. But for the *Euclid* and CSST surveys, multi-epoch observations based on their survey strategies (4 epochs in *NUV* and *y* bands and 2 epochs in the other filters for CSST; 3-4 epochs for *Euclid*) can help constrain RSG pulsations and thus better characterize the final evolutionary stage of massive stars.

In addition to *Euclid* and CSST, other telescopes will also play important roles in the search for SN progenitors, such as HST (e.g., Maund et al. 2005), JWST (e.g., Kilpatrick et al. 2025), LSST (Strotjohann et al. 2024) and Roman Space Telescope (Fraser et al. private communication). This wealth of data will enable the detection of SN progenitors over a wide wavelength range, at high spatial resolutions, down to deep detection limits, and across a large number of nearby galaxies, providing new insights into the evolution of massive stars and the origin of SNe.

Acknowledgements. The authors acknowledge the help from Prof. Mark Cropper, Dr. Mischa Schirmer, Dr. Erik Romelli, Dr. Paola Maria Battaglia, Dr. Chiara Sirignano and Dr. Eduardo Medinaceli for discussions and suggestions regarding the exposure time calculators of VIS and NISP of *Euclid*. NCS is funded by the China Manned Space Program No.CMS-CSST-2025-A14, the National Natural Science Foundation of China (NSFC) Grants No.12303051 and No.12261141690 and the Strategic Priority Research Program of the Chinese Academy of Sciences Grant No.XDB0550300. TMZ is funded by the NSFC Grant No.12233008. We acknowledge the use of the following software packages, programs, datasets, and model libraries: ASTROPY, CALIFA, DUSTMAPS, DUSTY, MARCS, PARSEC, PYSPHOT, SWIRE Template Library, and z0MGS.

Sánchez, S. F., García-Benito, R., Zibetti, S., et al. 2016, A&A, 594, A36
 Sánchez, S. F., Kennicutt, R. C., Gil de Paz, A., et al. 2012, A&A, 538, A8
 Sarangi, A., Dwek, E., & Arendt, R. G. 2018, ApJ, 859, 66
 Schlafly, E. F. & Finkbeiner, D. P. 2011, ApJ, 737, 103
 Schlegel, D. J., Finkbeiner, D. P., & Davis, M. 1998, ApJ, 500, 525
 Smartt, S. J. 2009, ARA&A, 47, 63
 Smartt, S. J. 2015, PASA, 32, e016
 Strotjohann, N. L., Ofek, E. O., Gal-Yam, A., et al. 2024, ApJ, 960, 72
 STScI Development Team. 2013, pysynphot: Synthetic photometry software package, Astrophysics Source Code Library, record ascl:1303.023
 Sukhbold, T., Ertl, T., Woosley, S. E., Brown, J. M., & Janka, H.-T. 2016, ApJ, 821, 38
 Suzuki, A. & Shigeyama, T. 2025, MNRAS, 543, 3929
 Van Dyk, S. D., Srinivasan, S., Andrews, J. E., et al. 2024, ApJ, 968, 27
 Van Dyk, S. D., Zheng, W., Fox, O. D., et al. 2014, AJ, 147, 37
 Van Dyk, S. D., Zheng, W., Maund, J. R., et al. 2019, ApJ, 875, 136
 Walcher, C. J., Wisotzki, L., Bekeraité, S., et al. 2014, A&A, 569, A1
 Walmswell, J. J. & Eldridge, J. J. 2012, MNRAS, 419, 2054
 Warren, M. L., Couch, S. M., O'Connor, E. P., & Morozova, V. 2020, ApJ, 898, 139
 Wei, C.-L., Li, G.-L., Fang, Y.-D., et al. 2025, arXiv e-prints, arXiv:2511.06970
 Woosley, S. E., Heger, A., & Weaver, T. A. 2002, Reviews of Modern Physics, 74, 1015
 Xiang, D., Mo, J., Wang, L., et al. 2024a, Science China Physics, Mechanics, and Astronomy, 67, 219514
 Xiang, D., Mo, J., Wang, X., et al. 2024b, ApJ, 969, L15
 Xiang, D., Wang, X., Mo, J., et al. 2019, ApJ, 871, 176
 z0MGS Team. 2019, z=0 Multiwavelength Galaxy Synthesis (z0MGS)
 Zhan, H. 2011, Scientia Sinica Physica, Mechanica & Astronomica, 41, 1441
 Zhan, H. 2021, Chinese Science Bulletin-Chinese, 66, 1290

References

Ban, Z., Li, X.-B., Yang, X., et al. 2025, arXiv e-prints, arXiv:2511.06936
 Bressan, A., Marigo, P., Girardi, L., et al. 2012, MNRAS, 427, 127
 Cardelli, J. A., Clayton, G. C., & Mathis, J. S. 1989, ApJ, 345, 245
 Chen, Y., Bressan, A., Girardi, L., et al. 2015, MNRAS, 452, 1068
 Chen, Y., Girardi, L., Bressan, A., et al. 2014, MNRAS, 444, 2525
 Crowther, P. A. 2007, ARA&A, 45, 177
 CSST Collaboration, Gong, Y., Miao, H., et al. 2025, arXiv e-prints, arXiv:2507.04618
 Davies, B. & Beasor, E. R. 2018, MNRAS, 474, 2116
 Davies, B. & Beasor, E. R. 2020, MNRAS, 493, 468
 Euclid Collaboration, Cropper, M. S., Al-Bahalwan, A., et al. 2025a, A&A, 697, A2
 Euclid Collaboration, Jahnke, K., Gillard, W., et al. 2025b, A&A, 697, A3
 Euclid Collaboration, Mellier, Y., Abdurro'uf, et al. 2025c, A&A, 697, A1
 Fu, X., Bressan, A., Marigo, P., et al. 2018, MNRAS, 476, 496
 Gilhuly, C. & Courteau, S. 2018, MNRAS, 477, 845
 Green, G. M. 2018, The Journal of Open Source Software, 3, 695
 Groh, J. H., Meynet, G., & Ekström, S. 2013, A&A, 550, L7
 Gustafsson, B., Edvardsson, B., Eriksson, K., et al. 2008, A&A, 486, 951
 Heger, A., Fryer, C. L., Woosley, S. E., Langer, N., & Hartmann, D. H. 2003, ApJ, 591, 288
 Ivezic, Z. & Elitzur, M. 1997, MNRAS, 287, 799
 Kashiyama, K. & Quataert, E. 2015, MNRAS, 451, 2656
 Kilpatrick, C. D., Drout, M. R., Auchettl, K., et al. 2021, MNRAS, 504, 2073
 Kilpatrick, C. D. & Foley, R. J. 2018, MNRAS, 481, 2536
 Kilpatrick, C. D., Foley, R. J., Jacobson-Galán, W. V., et al. 2023, ApJ, 952, L23
 Kilpatrick, C. D., Suresh, A., Davis, K. W., et al. 2025, ApJ, 992, L10
 Leonard, D. C. 2011, Ap&SS, 336, 117
 Leroy, A. K., Sandstrom, K. M., Lang, D., et al. 2019, ApJS, 244, 24
 Levesque, E. M., Massey, P., Olsen, K. A. G., et al. 2005, ApJ, 628, 973
 Levesque, E. M., Massey, P., Olsen, K. A. G., et al. 2006, ApJ, 645, 1102
 Lovegrove, E. & Woosley, S. E. 2013, ApJ, 769, 109
 Massey, P., DeGioia-Eastwood, K., & Waterhouse, E. 2001, AJ, 121, 1050
 Massey, P. & Olsen, K. A. G. 2003, AJ, 126, 2867
 Mathis, J. S., Rumpl, W., & Nordsieck, K. H. 1977, ApJ, 217, 425
 Maund, J. R., Fraser, M., Ergon, M., et al. 2011, ApJ, 739, L37
 Maund, J. R., Reilly, E., & Mattila, S. 2014, MNRAS, 438, 938
 Maund, J. R., Smartt, S. J., & Danziger, I. J. 2005, MNRAS, 364, L33
 Nadezhin, D. K. 1980, Ap&SS, 69, 115
 Niu, Z., Sun, N.-C., & Liu, J. 2024, ApJ, 970, L9
 Niu, Z., Sun, N.-C., Maund, J. R., et al. 2025, ApJ, 987, L10
 Niu, Z., Sun, N.-C., Maund, J. R., et al. 2023, ApJ, 955, L15
 Polletta, M., Tajer, M., Maraschi, L., et al. 2007, ApJ, 663, 81
 Pozzo, M., Meikle, W. P. S., Fassia, A., et al. 2004, MNRAS, 352, 457
 Salpeter, E. E. 1955, ApJ, 121, 161